Environmental Science & Technology

Article

pubs.acs.org/est

Manipulation of Persistent Free Radicals in Biochar To Activate Persulfate for Contaminant Degradation

Guodong Fang,[†] Cun Liu,[†] Juan Gao,[†] Dionysios D. Dionysiou,[§] and Dongmei Zhou*[,†]

[†]Key Laboratory of Soil Environment and Pollution Remediation, Institute of Soil Science, Chinese Academy of Sciences, Nanjing, 210008 Jiangsu, P. R. China

[§]Environmental Engineering and Science Program, University of Cincinnati, Cincinnati, Ohio 45221-0012, United States

Supporting Information

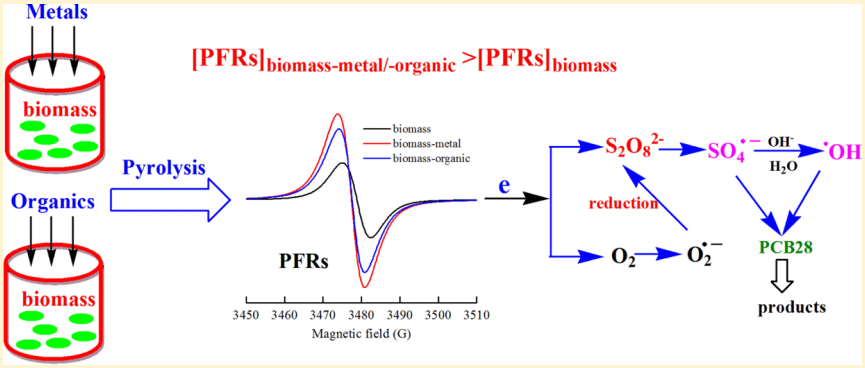

ABSTRACT: This study investigated the effects of metals (Fe^{3+}, Cu^{2+}, Ni^{2+}, and Zn^{2+}) and phenolic compounds (PCs: hydroquinone, catechol, and phenol) loaded on biomass on the formation of persistent free radicals (PFRs) in biochar. It was found that metal and phenolic compound treatments not only increased the concentrations of PFRs in biochar but also changed the types of PFRs formed, which indicated that manipulating the amount of metals and PCs in biomass may be an efficient method to regulate PFRs in biochar. These results provided direct evidence to elucidate the mechanism of PFR formation in biochar. Furthermore, the catalytic ability of biochar toward persulfate activation for the degradation of contaminants was evaluated. The results indicated that biochar activates persulfate to produce sulfate radicals ($SO_4^{\bullet-}$) and degraded polychlorinated biphenyls (PCBs) efficiently. It was found that both the concentration and type of PFRs were the dominant factors controlling the activation of persulfate by biochar and that superoxide radical anions account for 20−30% of sulfate radical generation in biochar/persulfate. This conclusion was supported by linear correlations between the concentration of PFRs consumed and the formation of $SO_4^{\bullet-}$ and between λ (λ = [formed sulfate radicals]/[consumed PFRs]) and g-factors. The findings of this study provide new methods to manipulate PFR concentration in biochar for the transformation of contaminants and development of new alternative activators for persulfate-based remediation of contaminated soils.

INTRODUCTION

In situ chemical oxidation (ISCO) technologies utilizing persulfate have been increasingly applied for the remediation of contaminated soil and groundwater in recent years.[1−3] There are large numbers of methods for persulfate activation to generate reactive $SO_4^{\bullet-}$ radicals including heat, UV, basic conditions (pH > 11), Fe^{2+}, zerovalent iron, metal oxides, and organic compounds (e.g., phenols and quinones), and all these methods have been extensively used in both laboratory research and field applications.[4−13] However, each activation method has its pros and cons when used in field applications. For example, heat is a simple and effective method for persulfate activation, but heat activation suffers from potential high costs as the temperature of soil and groundwater must be increased.[14] Fe^{2+} activation needs a high concentration of Fe^{2+} to prevent rapid conversion of Fe^{2+} to Fe^{3+}, which results from the scavenging of sulfate radicals ($SO_4^{\bullet-}$) by Fe^{2+} according to the following reactions and lowers the remediation efficiency of contaminants with persulfate[15]

$$Fe^{2+} + S_2O_8^{2-} \rightarrow SO_4^{\bullet-} + Fe^{3+} + SO_4^{2-} \quad 2.0 \times 10^1\ M^{-1}\ s^{-1},\ 22\ ^\circ C \tag{1}$$

$$Fe^{2+} + SO_4^{\bullet-} \rightarrow Fe^{3+} + SO_4^{2-} \quad 4.6 \times 10^9\ M^{-1}\ s^{-1},\ 22\ ^\circ C \tag{2}$$

Ethylenediaminetetraacetic acid (EDTA) has been successfully used as a chelating agent to avoid the rapid conversion of Fe^{2+} to Fe^{3+} and to provide a Fe^{2+}−Fe^{3+} redox couple to

Received: December 17, 2014
Revised: April 7, 2015
Accepted: April 13, 2015
Published: April 13, 2015

DOI: 10.1021/es5061512
Environ. Sci. Technol. 2015, 49, 5645−5653

facilitate persulfate activation; however, EDTA may compete with target contaminants for the consumption of sulfate radicals.[16−18] Base (pH > 11) may be used to activate persulfate to degrade contaminants efficiently and to neutralize the hydronium ions produced from persulfate decomposition; however, some recent studies have indicated that persulfate may decompose slowly at high pH.[19,20] Therefore, the development of efficient, low-cost, and environmentally friendly activators for the persulfate oxidation process is imperative and would be beneficial for devising effective and economically feasible remediation strategies for soil and groundwater heavily contaminated by organic pollutants.

Biochar derived from biomass waste is increasingly recognized as a multifunctional material for agricultural and environmental applications.[21,22] It has been reported that the application of biochar may improve soil fertility, raise agricultural productivity, increase holding capacities of soil nutrients and water, and reduce emissions of greenhouse gases.[23,24] Furthermore, biochar can be used as an environmentally engineered sorbent for immobilization of organic contaminants in water and soil.[25,26] Because of the abundance of feedstock materials, biochar is becoming a promising agent for large-scale environmental applications.[23] However, until now, few studies have focused on the ability of biochar to transform or catalytically degrade contaminants. We recently found that persistent free radicals (PFRs) in biochar catalyze H_2O_2 decomposition to form hydroxyl radicals ($^{\bullet}OH$), which then degraded polychlorinated biphenyls (PCBs) efficiently.[27] PFRs are resonance-stabilized and are formed from the thermal decomposition of organic compounds (e.g., catechol and hydroquinone) in the presence of metal oxides, which have half-lives in the order of hours to days under atmospheric conditions.[28−30] Similarly, Dong et al. found that dissolved organic matter (DOM) extracted from biochar contained PFRs, which reduced Cr(VI) and oxidized As(III) efficiently.[31] Liao et al. reported that the PFRs in biochar induced the formation of $^{\bullet}OH$ in the aqueous phase and significantly inhibited germination by retarding root and shoot growth in corn, wheat, and rice, respectively.[32] However, to date, the mechanism of PFR formation in biochar during the pyrolysis process has not been fully elucidated.

Similar to the activation of H_2O_2 by biochar, it is hypothesized that biochar may exhibit the ability to activate persulfate, since the activators for H_2O_2 are usually found to be effective for persulfate activation.[5] Therefore, the main objectives of this study were as follows: 1) to examine the mechanism of PFR formation in biochar during the pyrolysis process; 2) to testify the possibility of biochar to activate persulfate toward the degradation of a target pollutant; and 3) to explore the possible mechanism of persulfate activation by biochar. Moreover, the effects of pyrolysis temperature and time and organic and metal loadings on the PFR formation in biochar were studied. 2,4,4′-Trichlorobiphenyl (PCB28) was selected as the target contaminant because PCBs are an important group of persistent pollutants, and the mechanism of PCB28 degradation by $SO_4^{\bullet-}$ has been thoroughly investigated in our previous studies.[33]

MATERIALS AND METHODS

Materials. The chemicals used in this study are described in the Supporting Information (SI; Text S1), and the preparation and characterization of biochar are shown in Text S2, Table S1, and Figure S1. The biochar samples are referred to as P300, P400, P500, P600, and P700 for pine needles pyrolyzed at 300, 400, 500, 600, and 700 °C, respectively. The organic-loaded biochar samples are referred to as P400-HQ-1.0, P400-PH-1.0, and P400-CT-1.0 for pine needles loaded with 1.0 mM HQ, PH, and CT, respectively, pyrolyzed at 400 °C for 2 h. The metal-loaded biochar samples are referred to as P400-Fe-0.1, P400-Ni-0.1, P400-Cu-0.1, and P400-Zn-0.1 for pine needles loaded with 0.1 mM Fe^{3+}, Ni^{2+}, Cu^{2+}, and Zn^{2+}, respectively.

Degradation Experiments. The methods and procedures of free radical determination are provided in the SI (Text S3). Batch experiments were performed in the dark in 40 mL brown serum bottles sealed with Teflon Mininert containing 20 mL of reaction solution. Briefly, 20 mg of biochar was dispersed in a 19 mL aqueous solution of PCB28 (3.9 μM) at pH 7.4 (20 mM phosphate buffer) at 25 °C. After complete mixing, 1.0 mL of 0.16 M persulfate (the final concentration was 8.0 mM) was quickly added to initiate the reaction, and the mixtures were kept shaking at 150 rpm and 25 °C for different reaction times. Control experiments with biochar or persulfate alone were conducted under the same reaction conditions. Periodically, samples were removed for analysis and filtered through 0.22 μm PTFE membranes before the addition of 1.0 mL of ethanol into 4.0 mL of solution to quench the reaction. The sorption of PCB28 by the PTFE filter membrane was proved to be negligible by filtration of standard solutions (less than 5.0% of PCB28 (3.9 μM) adsorbed on PTFE membrane). Then, 1.0 mL of hexane was used to extract any remaining PCB28 in the quenched reaction solution. The hexane phase was analyzed by a gas chromatograph (GC/μECD, Aglient7890, USA) equipped with Ni^{63} electron capture detection (ECD).[47] The filtered biochar particles were collected and freeze-dried (Christ LD-1-2, Germany) and then divided into two parts. The first part was analyzed by EPR to quantify the PFR concentration remainin in the biochar after reaction; the second part was extracted with hexane to quantify the amount of PCB28 sorbed by the biochar. The recovery rate of PCB28 from biochar was in the range of 90−100%. To identify the types of products in the biochar during the pyrolysis process, the biochar was extracted with hexane/acetone (1:1, v/v) and analyzed with a gas chromatograph−mass spectrometer (GC−MS; GC Varian CP3800/MS Saturn2200, USA). All the experiments were carried out in triplicate, and results were reported as the mean with standard deviations. The other analysis methods used in this study are discussed in Text S4.

RESULTS AND DISCUSSION

Effects of Pyrolysis Temperature and Time on PFRs in Biochar. The effects of the pyrolysis temperature and time on the PFRs in biochar were examined with EPR spectroscopy. As shown in Figure 1a, a broad singlet EPR signal was observed in pine needle-derived biochar pyrolyzed at different temperatures for 1 h, while no EPR signal was observed in biomass without pyrolysis (Figure S2). The g-factors and $_{\Delta}H_{p\text{-}p}$ were 2.0048 and 7.0 G for P300, 2.0042 and 7.1 G for P400, 2.0038 and 6.0 G for P500, and 2.0037 and 7.1 G for P600, which are characteristic of oxygen-centered free radicals, indicating that oxygen-centered PFRs or carbon-centered PFRs with an adjacent oxygen atom formed in biochar during the pyrolysis process.[34] Since the g-factors for carbon-centered radicals were reported to be less than 2.0030, those for carbon-centered radicals with an adjacent oxygen atom were in the range of 2.0030−2.0040; while oxygen-centered radicals had g-factors

DOI: 10.1021/es5061512
Environ. Sci. Technol. 2015, 49, 5645−5653

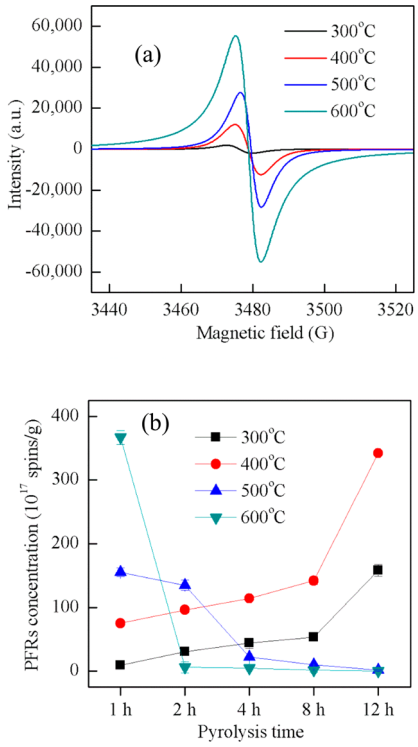

Figure 1. Effects of pyrolysis temperature and time on the formation of PFRs in biochar: (a) EPR spectra of 0.02 g of biochar particles with different pyrolysis temperatures for 1 h and (b) changes in PFR concentration as a function of pyrolysis temperature and time.

larger than 2.0040, and semiquinone radicals had *g*-factors larger than 2.0045.[27,29]

The PFR concentration as a function of pyrolysis temperature and time were then determined (Figure S3, Figure 1b). The PFR concentration increased rapidly from 8.96×10^{17} spins·g^{-1} to 158×10^{17} spins·g^{-1} for P300 and from 75.1×10^{17} spins·g^{-1} to 342×10^{17} spins·g^{-1} for P400, while it decreased markedly from 155×10^{17} spins·g^{-1} to 1.40×10^{17} spins·g^{-1} and from 367×10^{17} spins·g^{-1} to below the detection limit (BDL) for P500 and P600, respectively, under a prolonged pyrolysis time from 1 to 12 h. The EPR signal for P700 was too low to quantify the PFRs with increasing pyrolysis temperature up to 700 °C (P700 in Figure S3). Table S2 shows that the *g*-factors of PFR decreased as pyrolysis temperature and time increased. For example, the *g*-factor of all P300 treatments was larger than 2.0040, while the *g*-factor of all P600 treatments was less than 2.0040, which suggested that the types of PFR changed and exhibited the trend that oxygen-centered PFRs converted to carbon-centered PFRs with an adjacent oxygen atom as the pyrolysis time and temperature increased according to previous studies.[27,29,34] These results indicated that the concentrations and types of PFR formation were pyrolysis temperature and time-dependent. The best pyrolysis time for the formation of PFRs at relatively low temperature (300 and 400 °C) was 12 h, while at relatively high temperature (500, 600, and 700 °C) it was 1 h in the present study.

The decomposition of organic compounds (OCs) in biomass and PFRs was the likely reason for the temperature and time-dependent effects of PFR formation. OCs such as PCs in biomass are the main factor controlling the formation of PFRs in biochar, and PCs are precursors of PFR production.[27,34] These PCs would be decomposed as pyrolysis temperature and time increased,[35] which resulted in the reduction of PCs participating in the formation of PFRs. Moreover, PFRs also could be decomposed as pyrolysis temperature and time increased. Briefly, oxygen-centered PFRs were the predominant species at relatively low pyrolysis temperature and short pyrolysis time. As pyrolysis temperature and time increased, these oxygen-centered PFRs decomposed and converted to carbon-centered PFRs. For example, the oxygen-centered PFRs such as surface-bound semiquinone radical ($g > 2.0040$) would be decomposed to surface-bound phenoxyl radical ($g < 2.0040$) as the pyrolysis time and temperature increased.[29] Additionally, these oxygen-centered PFRs would also decay without PFRs conversion processes at relatively high temperature.

The decomposition of PFRs would change the diversity of products in extracts from biochar particles. Therefore, GC−MS was used to identify the diversity of OCs in extracts from biochar samples produced from different pyrolysis temperature and time. As shown in Figure S4, the eight major identified products in the extracts included *p*-cresol, 2-ethyl-phenol, 2,4-bis(1,1-dimethylethyl)phenol, tetradecenoic acid, oxacyclohep-tadecan-2-one, octadecanamide, retene, and 9-octadecenamide and were found for P300 pyrolyzing at 1 and 8 h. Similar products were also observed in P600 pyrolyzed for 2 h, but only three major products were observed in P600 pyrolyzed for 8 h; furthermore, most of these eight peaks disappeared with a further increase in pyrolysis temperature up to 700 °C for 1 h, which suggested that the diversities of OC in extracts were greatly reduced with increasing pyrolysis temperature and time. These results indicated that increasing pyrolysis temperature and time led to the decomposition of PFRs, which resulted in a decrease of diversities of products extracted from biochar particles.

According to Figures 1 and S4, it was hypothesized that OCs such as PCs in biomass would participate in the formation of PFRs in biochar. Dichloromethane is an efficient solvent to extract PCs from pine needles.[36] Therefore, to further test the role of OCs in pine needles in the formation of PFRs, pine needles were extracted with different organic solvents, including dichloromethane (DCM), dichloromethane/acetone (ACE, 1:1, v/v), ethanol (EtOH), and hexane (HEX)/acetone (1:1, v/v), and then were used to produce biochar. As shown in Figure S5, the concentrations of PFR in biochar decreased rapidly from 96.2×10^{17} spins·g^{-1} to 47.1×10^{17} spins·g^{-1}, to 26.9×10^{17} spins·g^{-1}, 16.4×10^{17} spins·g^{-1}, and 25.3×10^{17} spins·g^{-1} for EtOH, DCM, DCM/ACE, and HEX/ACE treatments, respectively, which suggested that the extraction of OCs from pine needles greatly reduced the formation of PFRs in biochar. The results indicated that OCs (e.g., PCs) would contribute to the formation of PFRs in biochar.

Manipulation of PFRs in Biochar with Metal and Organic Treatments. PCs and metals in biomass have been suggested to participate in the formation of PFRs in biochar, as found in our previous study (Figures S4 and S5, Scheme 1).[27] To elucidate the mechanism of PFR formation in biochar, pine needles loaded with different concentrations of PC (hydroquinone [HQ], phenol [PH], or catechol [CT]) or metals (Fe^{3+}, Ni^{2+}, Cu^{2+}, or Zn^{2+}) were pyrolyzed at 400 °C for 2 h and analyzed by EPR spectroscopy (Figures 2 and S6). As shown in Figure 2a, the PFR concentration increased sharply from 0.96×10^{19} spins·g^{-1} to 4.51×10^{19} spins·g^{-1} with 0.1 mM Fe^{3+} loading and then decreased to 1.55×10^{19} spins·g^{-1} with further increases in the concentration of Fe^{3+} from 0.1 to 10 mM. These results suggested that the concentration of PFRs

DOI: 10.1021/es5061512
Environ. Sci. Technol. 2015, 49, 5645−5653

Scheme 1. Proposed Pathway for PFR and Sulfate Radical Generation

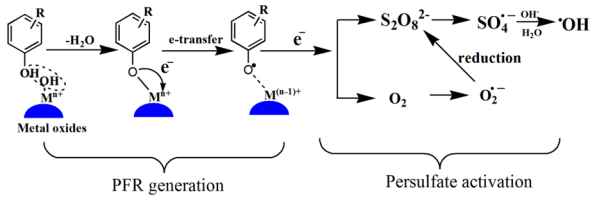

following Fe^{3+} treatment (Fe^{3+} concentration less than 10 mM) was markedly higher than without Fe^{3+} treatment. However, the PFR concentration following Fe^{3+} treatment was lower than without Fe^{3+} treatment when the Fe^{3+} concentration increased more than 20 mM. Similar results were also observed following other metal treatments. The concentrations of PFRs in biochar were 52.1×10^{19} spins·g^{-1}, 21.2×10^{19} spins·g^{-1}, and 4.12×10^{19} spins·g^{-1} for 0.1 mM Ni^{2+}, Cu^{2+}, and Zn^{2+}, respectively, while these concentrations decreased to 33.2×10^{19} spins·g^{-1}, 19.2×10^{19} spins·g^{-1}, and 3.23×10^{19} spins·g^{-1} when the corresponding metal concentrations increased up to 2.0 mM (Figure 2b). Figures 2c and 2d show that the concentrations of PFRs increased rapidly from 0.96×10^{19} spins·g^{-1} to 8.32×10^{19} spins·g^{-1}, 20.1×10^{19} spins·g^{-1}, and 14.2×10^{19} spins·g^{-1} for 5.0 mM HQ, CT, and PH loadings, respectively. The concentration of PFRs increased rapidly as the HQ concentration increased from 0 to 5.0 mM but decreased significantly as the HQ concentration increased from 5.0 to 50 mM (Figure 2c). Similar results were also observed for CT and PH treatments (Figure 2d). In addition, Figures S7a–c present the effects of pyrolysis temperature and time on the PFRs in biochar produced following metal and organic treatment; the results were consistent with the above-mentioned without metal and organic treatments.

These results suggested that both metal and PC treatment increased the concentration of PFRs in biochar, indicating that metal and PC loading on biomass favored the formation of PFRs in biochar. However, the metal and PC load concentrations influenced PFR formation significantly. For example, maximum PFR concentrations were observed for 0.1 mM metal and 5.0 mM PC treatments, but the PFR concentration decreased with further increases in load concentrations. The possible reason was that transition metal ions exhibit a double-effect in the formation of PFRs during the pyrolysis processes. For biochar loaded at relatively low concentration of metals, transition metal ions accept electrons from phenolic compounds and favor the formation of PFRs. In contrast, for biochar loaded at relatively high concentration of metals, the excess transition metal ion would consume PFRs, since it has been well established that PFRs can act as an electron shuttle to mediate the reduction of transition metal ions (e.g., Fe^{3+}).[37−39] XRD analysis was used to investigate this process. As shown in Figure S8, the $FeCl_2$ and Fe_2O_3 were the dominant Fe-species in biochar produced from Fe^{3+} treatment. The results indicated that Fe^{2+} was formed during the pyrolysis process, which would be generated from the reduction reaction between Fe^{3+} and PFRs, since PFRs in biochar can act as an electron shuttle and mediate the reduction of metals.[37−39] Therefore, the reduction of Fe^{3+} by PFRs is a most likely reason for the decrease of PFRs concentration as Fe^{3+} loaded concentration increased. A similar explanation seems feasible for understanding the concentration effects of PCs loaded biochar samples, since PCs exhibited a similar ability to Fe^{3+} or Fe^{2+} to consume PFRs (oxidation or reduction).

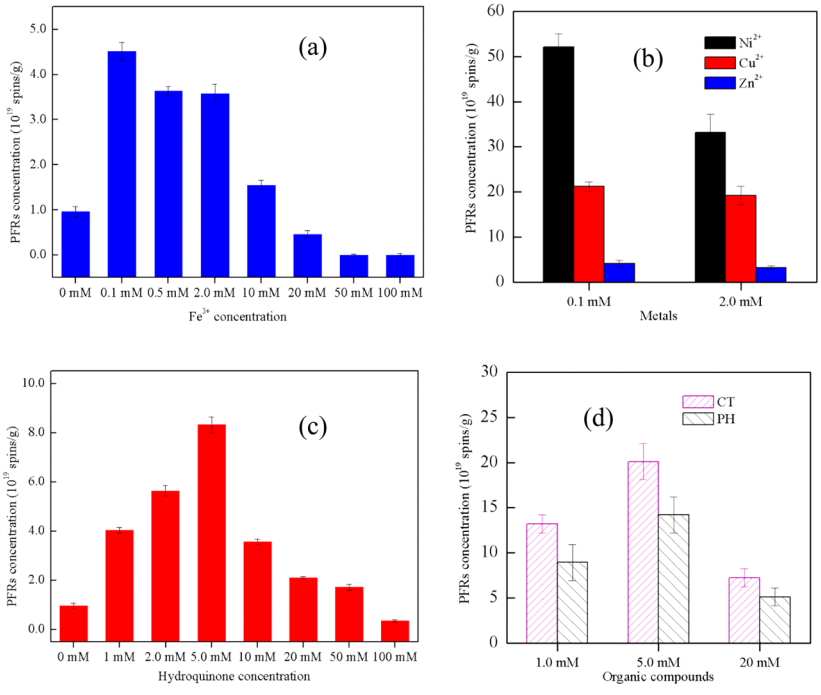

Figure 2. Effect of metal and organic loading on the concentration of PFRs in biochar: (a) changes in PFR concentration as a function of Fe^{3+} load concentration; (b) changes in PFR concentration as a function of Ni^{2+}, Cu^{2+}, and Zn^{2+} load concentration; (c) changes in PFR concentration as a function of HQ load concentration; and (d) changes in PFR concentration as a function of catechol (CT) and phenol (PH) load concentration. Reaction conditions: $[Fe^{3+}]_0$ = 0.1−100 mM; $[Ni^{2+}]_0 = [Cu^{2+}]_0 = [Zn^{2+}]_0$ = 0.1 mM (and 2.0 mM); $[HQ]_0$ = 1.0−100 mM; $[CT]_0 = [HQ]_0$ = 1.0 mM (5.0 and 20 mM); pyrolysis temperature of 400 °C for 2 h.

DOI: 10.1021/es5061512
Environ. Sci. Technol. 2015, 49, 5645−5653

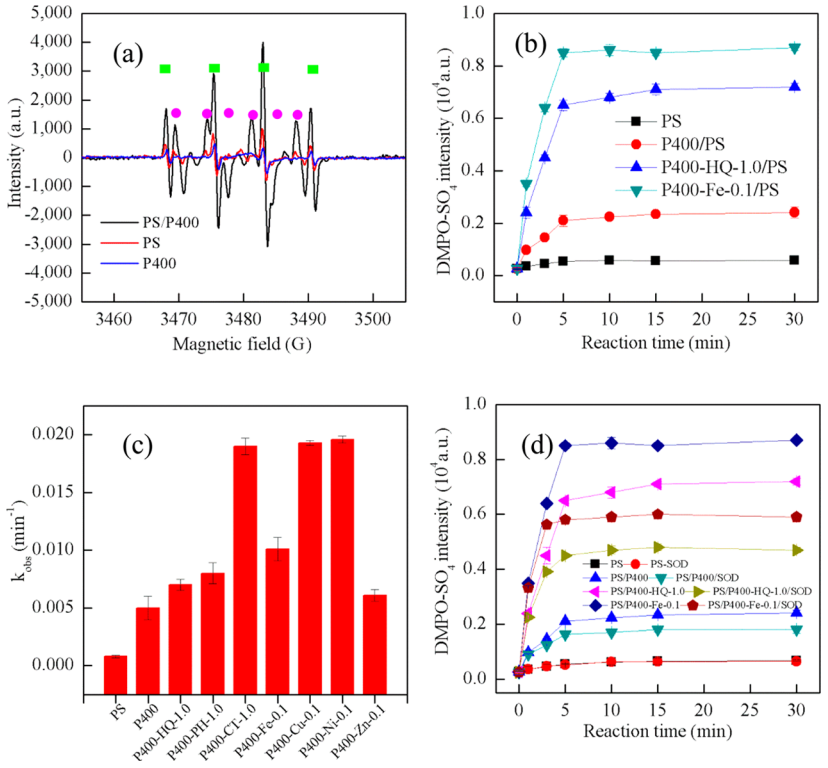

Figure 3. Activation of persulfate (PS) by biochar (pyrolysis time of 2 h) for PCB28 degradation: (a) EPR spectra of PS (red), P400 (blue) and P400/PS (black) in the presence of DMPO at 5.0 min; (b) changes in peak intensities of DMPO−SO_4 in the different biochar/PS systems; (c) pseudo-first-order rate constants (k_{obs}) for PCB28 degradation in the different biochar/PS systems; and (d) changes in peak intensities of DMPO−SO_4 in the different biochar/PS systems in the presence of SOD. Reaction conditions: $[PS]_0$ = 8.0 mM; $[P400]_0$ = $[P400\text{-}HQ\text{-}1.0]_0$ = $[P400\text{-}PH\text{-}1.0]_0$ = $[P400\text{-}CT\text{-}1.0]_0$ = $[P400\text{-}Fe\text{-}0.1]_0$ = $[P400\text{-}Ni\text{-}0.1]_0$ = $[P400\text{-}Cu\text{-}0.1]_0$ = $[P400\text{-}Zn\text{-}0.1]_0$ = 1.0 g·L^{-1}; $[DMPO]_0$ = 0.1 M; $[SOD]_0$ = 300 U·mL^{-1}; $[PCB28]_0$ = 3.9 μM; degradation time of 4 h, pH 7.4 (10 mM, phosphate-buffered saline) and 25 °C. Green square: DMPO−OH; pink circle: DMPO−SO_4.

Figure S9 shows that the *g*-factors of PFRs decreased from 2.0042 to 2.0032, from 2.0042 to 2.0039, from 2.0042 to 2.0036, and from 2.0042 to 2.0040 for 0.1 mM of Fe^{3+}, Ni^{2+}, Cu^{2+}, and Zn^{2+} treatments, respectively, while they increased from 2.0042 to 2.0052, 2.0048, and 2.0048 for 1.0 mM CT, PH, and HQ, respectively. The results suggested that metals or PCs loaded on the biomass changed the types of PFRs in biochar, which may influence the reactivity of the PFRs that mediate electron transfer processes. Figure 2 clearly indicated that manipulating the amount of metal species and PCs in biomass not only enhanced the formation of PFRs but also changed the types of PFRs in biochar, which provided direct evidence to support the pathway of PFR formation depicted in Scheme 1 as follows: phenolic compounds in biomass transfer electron to transition metals accompanied by the formation of surface-bound PFRs in biochar during the pyrolysis processes.

Activation of Persulfate by Biochar for PCB28 Degradation. To establish the possibility of persulfate (PS) activation by biochar, the activation of persulfate with different biochars was studied using EPR spectroscopy coupled with DMPO as a spin-trapping agent. This technique allowed us to identify the generation of sulfate and hydroxyl radicals, which are reportedly responsible for the degradation of contaminants in the PS system.[40] As shown in Figure 3a, mixing 8.0 mM PS with 0.1 M DMPO resulted in the formation of DMPO−SO_4 (six lines, 1:1:1:1:1:1) and DMPO−OH (four lines, 1:2:2:1) signals, which were identified from their hyperfine splitting constants ((DMPO−OH: $a_H = a_N$ = 14.7 G; DMPO−SO_4: a_N = 13.3 G, a_H = 9.5 G, a_H = 1.46 G, and a_H = 0.77 G) simulated with WinEPR Acquisition software. These results suggested the generation of $SO_4^{\bullet-}$ and $^{\bullet}OH$ in PS without biochar, although their peak intensities were relatively low (550 au for DMPO−SO_4 and 1500 au for DMPO−OH). In contrast, the peak intensities of DMPO−SO_4 and DMPO−OH increased sharply to 2100 au and 5500 au, respectively, with the addition of 1.0 g·L^{-1} P400, suggesting that the addition of P400 induced the generation of $SO_4^{\bullet-}$ and $^{\bullet}OH$ in P400/PS. Moreover, the DMPO−OH signal was observed in P400 suspensions without PS, possibly due to single electron transfer from the PFRs to oxygen, inducing the formation of $^{\bullet}OH$ via Fenton-like reactions.[41] These results indicated that P400 activated PS efficiently to produce sulfate radicals.

In the PS system, $SO_4^{\bullet-}$ was the predominant radical species, although $SO_4^{\bullet-}$ and $^{\bullet}OH$ usually coexisted as $^{\bullet}OH$ derives from the reaction of $SO_4^{\bullet-}$ with OH^- or H_2O and both accounted for the degradation of contaminants.[7] Therefore, the peak intensities of DMPO−SO_4 were used to indicate the concentrations of $SO_4^{\bullet-}$ and the activation ability of biochar in the biochar/PS system. The changes in the peak intensities of DMPO−SO_4 as a function of reaction time were determined (Figure 3b). The peak intensities of DMPO−SO_4 increased rapidly from 260 au to 2100 au for P400, from 260 au to 6500 au for P400-HQ-1.0, and from 260 au to 8500 au for P400-Fe-0.1 within 5 min and changed slightly as the reaction time increased up to 30 min. The peak intensities of DMPO−SO_4 in P400-HQ-1.0/PS and P400-Fe-0.1/PS were significantly higher than in P400/PS, which indicated that biochar produced from metal and organic treatments was more reactive than biochar

DOI: 10.1021/es5061512
Environ. Sci. Technol. 2015, 49, 5645−5653

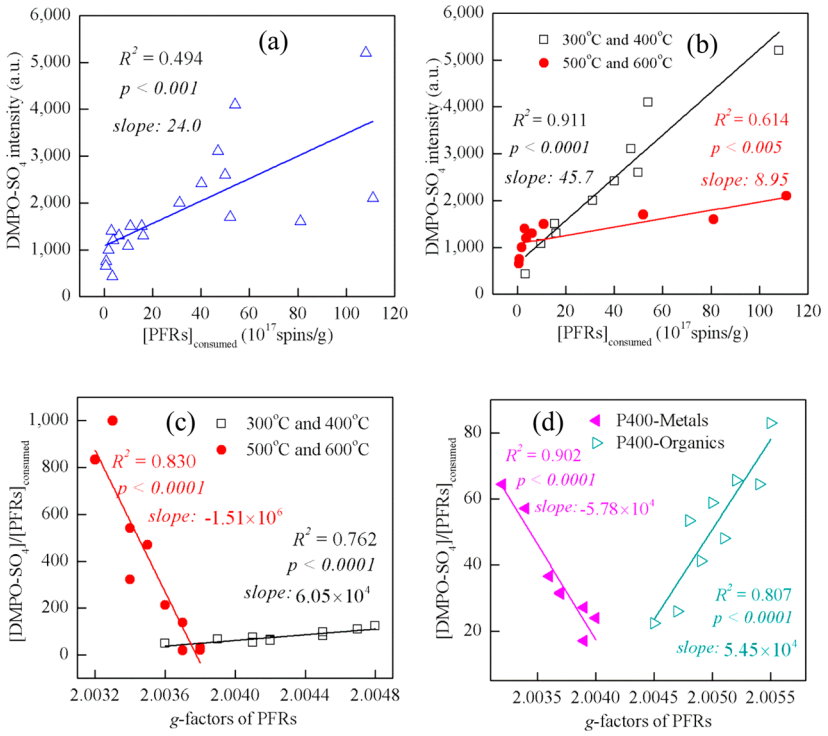

Figure 4. Correlation between PFRs consumed and sulfate radical formation (a) and (b) correlation between the concentration of PFRs consumed and the peak intensities of DMPO−SO_4 formed; (c) and (d) correlations between the values of the normalized concentrations of PFRs consumed and peak intensities of DMPO−SO_4 and the *g*-factors of corresponding PFRs. All the data presented were obtained from Table S3 described in the SI and resulted from the activation of persulfate by different biochar samples.

without treatment for PS activation. Similar results were also observed following other metal and organic treatments (Figure S10 and Table S3). Moreover, Table S3 shows that the PFR concentration in biochar decreased markedly after reaction with PS for 30 min, which suggested that the PFRs were consumed during the activation process.

Furthermore, PS activation by biochar for the degradation of PCB28 was studied. Figure S11a showed that 70−100% of PCB28 (3.9 μM) disappeared in biochar/PS, while only 20% of PCB28 was degraded in PS (8.0 mM) alone within 240 min. Moreover, ∼15% of PCB28 removal was attributed to the adsorption on P400 (data not shown). The degradation of PCB28 can be well described by pseudo-first-order reaction eqs (Figure S11). The pseudo-first-order constants (k_{obs}) were 0.005 min^{-1} for P400, 0.007 min^{-1} for P400-HQ-1.0, 0.008 min^{-1} for P400-PH-1.0, 0.019 min^{-1} for P400-CT-1.0, 0.010 min^{-1} for P400-Fe-0.1, 0.019 min^{-1} for P400-Cu-0.1, 0.020 min^{-1} for P400-Ni-0.1, and 0.006 min^{-1} for P400-Zn-0.1 (Figure 3c). These results indicated that the activation of PS by biochar degraded PCB28 efficiently, but the activation ability of different biochar samples varied significantly.

Possible Mechanism of Persulfate Activation by Biochar. A number of previous studies have reported that PFRs and biochar can act as electron shuttles to mediate electron transfer reactions.[37,38,42,43] For example, Dellinger and co-workers demonstrated that PFRs in combustion products can transfer an electron to molecular oxygen to form the superoxide radical ion, which then induces Fenton reactions to produce $^{\bullet}OH$.[41−43] PFRs in biochar can catalyze H_2O_2 decomposition to induce the formation of hydroxyl radicals via a single electron transfer process.[27] More recently, the redox ability of biochar was systematically assessed with electrochemical methods,[37] and it was found that biochar can act as an electron shuttle between bacteria and Fe(III) minerals.[38] Furthermore, results in Figure 2 provide direct evidence to support the pathway of PFRs formation depicted in Scheme 1. On the basis of the literature and the observations made here, similar to single electron transfer from PFRs to H_2O_2 to induce the formation of $^{\bullet}OH$,[27] it was hypothesized that the electron transfer from PFRs to persulfate is the most likely mechanism of PS activation by biochar (Scheme 1) as follows: 1) $S_2O_8^{2-}$ accepts an electron from PFRs to decompose into $SO_4^{\bullet-}$; 2) PFRs transfer an electron to oxygen to produce superoxide radical anion (SRA), and then SRA reacts with $S_2O_8^{2-}$ also to produce $SO_4^{\bullet-}$; 3) $SO_4^{\bullet-}$ reacts with H_2O or OH^- to yield to $^{\bullet}OH$, and both $SO_4^{\bullet-}$ and $^{\bullet}OH$ are responsible for PCB28 degradation.

Role of Superoxide Radical Anions and Fe-Species. The in situ generation of hydroxyl radicals is usually dependent on superoxide radical anions (SRAs).[44,45] Figure 3a shows the $^{\bullet}OH$ formation in biochar suspensions without the addition of PS and indicates that SRAs are formed in the biochar suspensions. Moreover, it has been reported that SRAs attached to the surface of solid particles can reduce persulfate ions to produce $SO_4^{\bullet-}$.[46] Therefore, the reduction of persulfate ions by SRAs could be another important pathway for $SO_4^{\bullet-}$ generation from PS activation by biochar. Superoxide dismutase (SOD) was used as a scavenger to assess the role of SRAs in this process. As shown in Figure 3d, peak intensities of DMPO−SO_4 in PS changed slightly in the presence of 300 U·mL^{-1} SOD, which suggested that SOD had limited effects on the formation of DMPO−SO_4 from the reaction of DMPO and $SO_4^{\bullet-}$. In contrast, the peak intensities of DMPO−SO_4 decreased significantly from 2100 au to 1500 au for PS/P400, from 6500 au to 4500 au for PS/P400-HQ, and from 8800 au

DOI: 10.1021/es5061512
Environ. Sci. Technol. 2015, 49, 5645−5653

to 5800 au for PS/P400-Fe in the presence of 300 U·mL^{-1} SOD after 5.0 min, which indicated that the generation of $SO_4^{\bullet-}$ in biochar/PS was greatly inhibited by SOD. An explanation for this behavior is that SOD quenched SRAs, resulting in the reduced formation of $SO_4^{\bullet-}$ from the reaction of persulfate ions and SRAs. These results showed that the DMPO−SO_4 peak intensities decreased 20−30% (calculated from Figure 3d) with the addition of SOD, which indicated that the SRAs contributed about 20−30% of $SO_4^{\bullet-}$ generation in the biochar/PS system.

It has been demonstrated that some metal oxides such as Fe(III) and Mn(IV) oxides catalyze the decomposition of persulfate to produce sulfate radicals.[8,11,47] Biochar, especially biochar produced from metal-loaded biomass, contains metal oxides. For example, the Fe, Zn, and Mn contents in biochar without metal treatment were 1.5−2.2 g·kg^{-1}, 0.061−0.075 g·kg^{-1}, and 0.11−0.19 g·kg^{-1}, respectively (data not shown). For Fe^{3+} treatment, the Fe content was about 25.0−124 g·kg^{-1} in biochar samples. XRD analysis showed the formation of Fe^{2+}-species and Fe_2O_3 in biochar with Fe^{3+} loaded treatments (Figure S8). Consequently, it was hypothesized that Fe-species in biochar would also contribute to persulfate activation and PCB28 degradation.

To investigate this possibility, the activation of persulfate by commercial Fe_3O_4 and Fe_2O_3 for PCB28 degradation was examined. The amount of Fe_2O_3 (0.176 g/L, 2.2 mM Fe^{3+}) and Fe_3O_4 (0.171 g/L, 2.2 mM Fe = 1.46 mM Fe^{3+} + 0.74 mM Fe^{2+}) used in this experiment was equal to the maximum Fe content (124 g/kg, 1.0 g/L biochar contains about 2.2 mM Fe) in biochar. As shown in Figure S12, 49% and 37% of 3.9 μM PCB28 degraded in the Fe_3O_4/PS and Fe_2O_3/PS systems, respectively, while 20% of PCB28 was degraded in PS alone, and less than 8% of PCB28 sorbed on these metal oxides within 240 min, which suggested that Fe_3O_4 and Fe_2O_3 activation accounted for about 20% and 10% of PCB28 degradation, respectively. These results indicated that Fe-species in biochar would contribute for persulfate activation and PCB28 degradation, especially for biochar produced from Fe^{3+} loaded treatments, but for most of biochar without Fe^{3+} loaded treatments, this contribution was limited, since the content of Fe was extremely low in these biochar particles.

Role of PFRs. As described in Scheme 1, PFRs were the primary electron donors, which transfer electrons to persulfate ions to induce the formation of sulfate radical. To assess the role of PFRs in PS activation by biochar, correlations between the concentration of PFRs consumed and the peak intensities of sulfate radical formed were analyzed. As shown in Figure 4a, a positive correlation between the concentration of PFRs consumed and the peak intensities of DMPO−SO_4 was observed, but the correlation coefficient was only 0.493 (p < 0.001), indicating that the concentration of PFRs was not the unique factor controlling the formation of $SO_4^{\bullet-}$ in the biochar/persulfate system. The types of PFR would be another important factor to affect the reactivity of PFR with persulfate for $SO_4^{\bullet-}$ generation, since the g-factors of PFR varied significantly in Figure 4a (Table S2). Briefly, these PFRs could be divided into two groups according to their g-factors: carbon-centered PFRs with an adjacent oxygen atom for P500 and P600 (denoted as "Group I", g-factor of 2.0030−2.0040) and oxygen-centered PFRs for P300 and P400 (Group II, g-factor larger than 2.0040). To assess the effects of PFR types on $SO_4^{\bullet-}$ formation of in biochar/persulfate, the concentrations of PFRs consumed in Group I and Group II were correlated with the corresponding generated peak intensities of DMPO−SO_4 (Figure 4b). The correlation coefficients and slopes were 0.911, 45.7, and 0.614, 8.95 for Group II and Group I, respectively, which suggested that with production of the same concentration of $SO_4^{\bullet-}$, more PFRs would be consumed for Group I than for Group II. These results indicate that oxygen-centered PFRs (Group II) are more reactive than carbon-centered PFRs with adjacent oxygen (Group I) toward persulfate for the generation of sulfate radical.

To further understand the effects of the types of PFR on the formation of $SO_4^{\bullet-}$, the peak intensities of DMPO−SO_4 were normalized with the concentration of the PFRs consumed (the normalized value was denoted as λ = [DMPO−SO_4]/$[PFRs]_{consumed}$) and then correlated with corresponding g-factors. As shown in Figure 4c, a negative correlation was found between λ and the g-factor with a correlation coefficient (R^2) and slope of 0.83 and -1.51×10^6 for Group I; however, a positive correlation was observed between λ and the g-factor for Group II (R^2 = 0.762, slope of 6.05×10^4). The results showed that λ values increased with increasing g-factors for Group II and decreased with decreasing g-factors for Group I. For Group I (carbon-centered PFRs with an adjacent oxygen atom), the closer the g-factor to the carbon-centered radicals (g < 2.0030), the higher concentration of PFRs consumed to generate the same amount of sulfate radical, which indicated that carbon-centered PFRs with an adjacent oxygen atom were more efficient than carbon-centered PFRs toward persulfate for the production of sulfate radical. For Group II (oxygen-centered PFRs), the closer the g-factor to the semiquinone radicals (g > 2.0045), the higher concentration of PFRs consumed to generate the same amount of sulfate radical, suggesting that the ability of oxygen-centered PFRs toward persulfate to generate sulfate radical decreased with increasing their g-factors. Overall, most of the λ values for Group I were markedly higher than those for Group II, which further indicated that oxygen-centered PFRs were more efficient than carbon-centered PFRs toward persulfate for $SO_4^{\bullet-}$ generation. The results are consistent with the correlation analysis presented in Figure 4b.

Similar results were also observed in the activation of PS by metal- and organic-loaded biochar (Table S2, Figure 4d). The g-factors were ranged from 2.0030 to 2.0040 for metal-loaded biochar, while were larger than 2.0040 for PC-loaded biochar, which indicated that carbon-centered PFRs with an adjacent oxygen atom (Group I) and oxygen-centered PFRs (Group II) were present in metal-loaded and PC-loaded biochars, respectively. A negative correlation (R^2 = 0.902) between λ and the g-factor was obtained when the g-factor was less than 2.0040 (metal-loaded treatments, Group I), while a positive correlation between λ and the g-factor was observed when the g-factor was larger than 2.0040 (organic loaded treatments, Group II). The trend of λ changes as a function of g-factor was the same as that shown in Figure 4c. However, the λ value was markedly lower than that of biochar produced without loading treatments, which suggested that biochar produced from metal or PC-loaded treatments was more efficient than biochar produced without treatment toward $SO_4^{\bullet-}$ generation in the biochar/persulfate system. These results indicated that both the concentration and type of PFR influenced the activation ability of PFRs in biochar, and PFRs were the primary factor for persulfate activation by biochar.

Environmental Implications. This study found that the manipulation of metal and organic concentrations in biomass significantly changed the concentrations and g-factors of PFRs

DOI: 10.1021/es5061512
Environ. Sci. Technol. 2015, 49, 5645−5653

in biochar, which provided direct evidence for the identification of the pathway by which PFRs are formed during the pyrolysis of biomass. Moreover, PFRs in biochar exhibited an excellent ability to activate persulfate for the degradation of contaminants. Both the concentration and type of PFR influenced the generation of sulfate radicals from the biochar/PS system. The findings from this study have significant implications for the transformation of contaminants by biochar and for the use of persulfate in the remediation of contaminated soils.

First, this study provides a new method to regulate the concentration and type of PFR in biochar, which could improve the catalytic reactivity of biochar since PFRs were found to be efficient shuttle mediating electron transfer reactions.[36,42] This means that biochar exhibited the ability to induce the formation of reactive oxygen species (ROS) and transform contaminants efficiently under specific geochemical conditions (e.g., O_2 and S^{2-}).[32,48,49] Consequently, it can be concluded that the application of biochar to soils can not only change the physicochemical properties of soil but also influence soil biogeochemistry processes including PFRs in biochar acting as terminal electron acceptors in anaerobic respiration,[37] mitigating the nitrous oxide emissions from soils by inducing the formation ROS,[50,51] and mediating the reductive transformation of pollutants in the presence of sulfide in soils.[52] Second, this study would develop an alternative activator for persulfate decomposition in persulfate-based remediation of contaminated soils. Moreover, combination of biochar sorption with the persulfate-mediated oxidation of contaminants is an excellent strategy for the remediation of contaminated soil, especially for organic-polluted soil. Finally, our study provides a new strategy for the reuse of hyperaccumulator biomass in the phytoremediation of heavy metal from soil. For example, we can pyrolyze hyperaccumulator biomass to prepare new catalytic materials, which can be further used in the catalytic decomposition of oxidants (e.g., hydrogen peroxide and persulfate) for the degradation of pollutants and the remediation of contaminated soil.

■ ASSOCIATED CONTENT

Supporting Information

Characteristics of biochar (FTIR, element composition, and EPR spectra), changes in concentrations of PFRs, and degradation kinetics of PCB28. This material is available free of charge via the Internet at http://pubs.acs.org.

■ AUTHOR INFORMATION

Corresponding Author

*Phone: 86 25 86881180. Fax: 86 25 86881180. E-mail: dmzhou@issas.ac.cn.

Notes

The authors declare no competing financial interest.

■ ACKNOWLEDGMENTS

This work was supported by the grants from the National Key Basic Research Program of China (2013CB934303 and 2014CB441105), the National Natural Science Foundation of China (41401252), the Natural Science Foundation of Jiangsu Province of China (BK20141047), and the One Hundred Person Project of the Chinese Academy of Sciences. The authors also thank the anonymous reviewers for their invaluable comments and suggestions to improve the quality of the paper.

■ REFERENCES

(1) Dahmani, M. A.; Huang, K. H.; Hoag, G. E. Sodium persulfate oxidation for the remediation of chlorinated solvents (USEPA superfund innovative technology evaluation program). *Water, Air, Soil. Pollut.* **2006**, *6*, 127−141.

(2) Anipsitakis, G. P.; Dionysiou, D. D. Degradation of contaminants in water with sulfate radicals generated by the conjunction of peroxymonosulfate with cobalt. *Environ. Sci. Technol.* **2003**, *37*, 4790−4797.

(3) Anipsitakis, G. P.; Dionysiou, D. D.; Gonzalez, M. A. Cobalt-mediated activation of peroxymonosulfate and sulfate radical attack on phenolic compounds: Implications of chloride ions. *Environ. Sci. Technol.* **2006**, *40*, 1000−1007.

(4) Waldemer, R. H.; Tratnyek, P. G.; Johnson, R. L.; Nurmi, J. T. Oxidation of chlorinated ethenes by heat-activated persulfate: kinetics and products. *Environ. Sci. Technol.* **2007**, *41*, 1010−1015.

(5) Liang, C.; Bruell, C. J.; Marley, M. C.; Sperry, K. L. Thermally activated persulfate oxidation of trichloroethylene (TCE) and 1,1,1-trichloroethane (TCA) in aqueous systems and soil slurries. *Soil Sediment Contam.* **2003**, *12*, 207−228.

(6) Guan, Y. H.; Ma, J.; Li, X. C.; Fang, J. Y.; Chen, L. W. Influence of pH on the formation of sulfate and hydroxyl radicals in the UV/peroxymonosulfate system. *Environ. Sci. Technol.* **2011**, *45*, 9308−9314.

(7) Liang, C.; Bruell, C. J.; Marley, M. C.; Sperry, K. L. Persulfate oxidation for in situ remediation of TCE. I. Activated by ferrous ion with and without a persulfate-thiosulfate redox couple. *Chemosphere* **2004**, *55*, 1213−1223.

(8) Teel, A. L.; Ahmad, M.; Watts, R. J. Persulfate activation by naturally occurring trace minerals. *J. Hazard. Mater.* **2011**, *196*, 153−159.

(9) Zhang, T.; Chen, Y.; Wang, Y.; Roux, J. L.; Yang, Y.; Croué, J. An efficient peroxydisulfate activation process not relying on sulfate radical generation for water pollutant degradation. *Environ. Sci. Technol.* **2014**, *48*, 5868−5875.

(10) Fang, G. D.; Dionysiou, D. D.; Al-Abed, S. R.; Zhou, D. M. Superoxide radical driving the activation of persulfate by magnetite nanoparticles: Implications for the degradation of PCBs. *Appl. Catal., B* **2013**, *129*, 325−332.

(11) Liu, H. Z.; Bruton, T. A.; Doyle, F. M.; Sedlak, D. L. In situ chemical oxidation of contaminated groundwater by persulfate: decomposition by Fe(III)- and Mn(IV)-containing oxides and aquifer materials. *Environ. Sci. Technol.* **2014**, *48*, 10330−10336.

(12) Ahmad, M.; Teel, A. L.; Watts, R. J. Mechanism of persulfate activation by phenols. *Environ. Sci. Technol.* **2013**, *47*, 5864−5871.

(13) Yuan, S. H.; Liao, P.; Alshawabkeh, A. N. Electrolytic manipulation of persulfate reactivity by iron electrodes for trichloroethylene degradation in groundwater. *Environ. Sci. Technol.* **2014**, *48*, 656−663.

(14) Tsitonaki, A.; Petri, B.; Crimi, M.; Mosbæk, H.; Siegrist, R. L.; Bjerg, P. L. In situ chemical oxidation of contaminated soil and groundwater using persulfate: a review. *Crit. Rev. Environ. Sci. Technol.* **2010**, *40*, 55−91.

(15) Al-Shamsi, M. A.; Thomson, N. R. Treatment of organic compounds by activated persulfate using nanoscale zerovalent iron. *Ind. Eng. Chem. Res.* **2013**, *52*, 13564−13571.

(16) Ahmad, M.; Teel, A. L.; Furman, O. S.; Reed, J. I.; Watts, R. J. Oxidative and reductive pathways in iron-ethylenediaminetetraacetic acid-activated persulfate systems. *J. Environ. Eng.* **2012**, *138*, 411−418.

(17) Liang, C. J.; Liang, C. P.; Chen, C. C. pH dependence of persulfate activation by EDTA/Fe(III) for degradation of trichloroethylene. *J. Contam. Hydrol.* **2009**, *106*, 173−182.

(18) Yan, D. Y. S.; Lo, I. M. C. Removal effectiveness and mechanisms of naphthalene and heavy metals from artificially contaminated soil by iron chelate-activated persulfate. *Environ. Pollut.* **2013**, *178*, 15−22.

(19) Furman, O. S.; Teel, A. L.; Watts, R. J. Mechanism of base activation of persulfate. *Environ. Sci. Technol.* **2010**, *44*, 6423−6428.

DOI: 10.1021/es5061512
Environ. Sci. Technol. 2015, 49, 5645−5653

(20) Crimi, M. L.; Taylor, J. Experimental evaluation of catalyzed hydrogen peroxide and sodium persulfate for destruction of BTEX contaminants. *Soil Sediment Contam.* **2007**, *16*, 29−45.
(21) Chen, Z.; Chen, B.; Chiou, C. T. Fast and slow rates of naphthalene sorption to biochars produced at different temperatures. *Environ. Sci. Technol.* **2012**, *46*, 11104−11111.
(22) Li, F.; Cao, X.; Zhao, L.; Wang, J.; Ding, Z. Effects of mineral additives on biochar formation: carbon retention, stability, and properties. *Environ. Sci. Technol.* **2014**, *48*, 11211−11217.
(23) Manyà, J. J. Pyrolysis for Biochar Purposes: A review to establish current knowledge gaps and research needs. *Environ. Sci. Technol.* **2012**, *46*, 7939−7954.
(24) Lehmann, J. A handful of carbon. *Nature* **2007**, *447*, 143−144.
(25) Yao, Y.; Gao, B.; Chen, J. J.; Yang, L. Y. Engineered biochar reclaiming Phosphate from aqueous solutions: mechanisms and potential application as a slow-release fertilizer. *Environ. Sci. Technol.* **2013**, *47*, 8700−8708.
(26) Chen, B.; Chen, Z.; Lv, S. A novel magnetic biochar efficiently sorbs organic pollutants and phosphate. *Bioresour. Technol.* **2011**, *102*, 716−723.
(27) Fang, G. D.; Gao, J.; Liu, C.; Dionysiou, D. D.; Wang, Y.; Zhou, D. M. Key role of persistent free radicals in hydrogen peroxide activation by biochar: implications to organic contaminant degradation. *Environ. Sci. Technol.* **2014**, *48*, 1902−1910.
(28) Lomnicki, S.; Truong, H.; Vejerano, E.; Dellinger, B. Copper oxide-based model of persistent free radical formation on combustion-derived particulate matter. *Environ. Sci. Technol.* **2008**, *42*, 4982−4988.
(29) Vejerano, E.; Lomnicki, S.; Dellinger, B. Formation and stabilization of combustion-generated environmentally persistent free radicals on an $Fe(III)_2O_3$/ silica surface. *Environ. Sci. Technol.* **2010**, *45*, 589−594.
(30) Gehling, W.; Dellinger, B. Environmentally persistent free radicals and their lifetimes in PM2.5. *Environ. Sci. Technol.* **2013**, *47*, 8172−8178.
(31) Dong, X.; Ma, L. Q.; Gress, J.; Harris, W.; Li, Y. Enhanced Cr(VI) reduction and As(III) oxidation in ice phase: Important role of dissolved organic matter from biochar. *J. Hazard. Mater.* **2014**, *267*, 62−70.
(32) Liao, S.; Pan, B.; Li, H.; Zhang, D.; Xing, B. Detecting free radicals in biochars and determining their ability to inhibit the germination and growth of corn, wheat and rice seedlings. *Environ. Sci. Technol.* **2014**, *48*, 8581−8587.
(33) Fang, G. D.; Dionysiou, D. D.; Zhou, D. M.; Wang, Y.; Zhu, X. D.; Fan, J. X.; Cang, L.; Wang, Y. J. Transformation of polychlorinated biphenyls by persulfate at ambient temperature. *Chemosphere* **2013**, *90*, 1573−1580.
(34) Dela Cruz, A. L. N.; Cook, R. L.; Lomnicki, S. M.; Dellinger, B. Effect of low temperature thermal treatment on soils contaminated with pentachlorophenol and environmentally persistent free radicals. *Environ. Sci. Technol.* **2012**, *46*, 5971−5978.
(35) Lomnicki, S.; Truong, H.; Dellinger, B. Mechanisms of product formation from the pyrolytic thermal degradation of catechol. *Chemosphere* **2008**, *73*, 629−633.
(36) Zhang, J. M.; Shi, X. F.; Ma, Q. H.; He, F. J.; Fan, B.; Wang, D. D.; Liu, D. Y. Chemical constituents from pine needles of *Cedrus deodara*. *Chem. Nat. Compd.* **2011**, *47*, 272−274.
(37) Klüpfel, L.; Keiluweit, M.; Kleber, M.; Sander, M. Redox properties of plant biomass-derived black carbon (biochar). *Environ. Sci. Technol.* **2014**, *48*, 5601−5611.
(38) Kappler, A.; Wuestner, M. L.; Ruecker, A.; Harter, J.; Halama, M.; Sebastian Behrens, S. Biochar as an electron shuttle between bacteria and Fe(III) minerals. *Environ. Sci. Technol. Lett.* **2014**, *1*, 339−344.
(39) Xu, Y.; Lou, Z.; Yi, P.; Chen, J.; Ma, X.; Wang, Y.; Li, M.; Chen, W.; Liu, Q.; Zhou, J.; Zhang, J.; Qian, R. Improving abiotic reducing ability of hydrothermal biochar by low temperature oxidation under air. *Bioresour. Technol.* **2014**, *172*, 212−218.
(40) Fang, G. D.; Dionysiou, D. D.; Wang, Y.; Al-Abed, S. R.; Zhou, D. M. Sulfate radical based degradation of polychlorinated biphenyls: effects of chloride ion and reaction kinetics. *J. Hazard. Mater.* **2012**, *227/228*, 394−401.
(41) Khachatryan, L.; McFerrin, C. A.; Hall, R. W.; Dellinger, B. Environmentally persistent free radicals (EPFRs). 3. Free versus bound hydroxyl radicals in EPFR aqueous solutions. *Environ. Sci. Technol.* **2014**, *48*, 9220−9226.
(42) Khachatryan, L.; Vejerano, E.; Lomnicki, S.; Dellinger, B. Environmentally persistent free radicals (EPFRs). 1. Generation of reactive oxygen species in aqueous solutions. *Environ. Sci. Technol.* **2011**, *45*, 8559−8566.
(43) Dela Cruz, A. L. N.; Gehling, W.; Lomnicki, S.; Cook, R. L.; Dellinger, B. Detection of environmentally persistent free radicals at a superfund wood treating site. *Environ. Sci. Technol.* **2011**, *45*, 6356−6365.
(44) Joo, S. H.; Feitz, A. J.; Sedlak, D. L.; Waite, T. D. Quantification of the oxidizing capacity of nanoparticulate zero-valent iron. *Environ. Sci. Technol.* **2005**, *39*, 1263−1268.
(45) Katsoyiannis, I. A.; Ruettimann, T.; Hug, S. J. pH dependence of Fenton reagent generation and As(III) oxidation and removal by corrosion of zero valent iron in aerated water. *Environ. Sci. Technol.* **2008**, *42*, 7424−7430.
(46) Furman, O. Reactivity of oxygen species in homogeneous and heterogeneous aqueous environments, Ph.D. Dissertation, Washington State University, WA, 2009.
(47) Ahmad, M.; Teel, A. L.; Watts, R. J. Persulfate activation by subsurface minerals. *J. Contam. Hydrol.* **2010**, *115*, 34−45.
(48) Xu, W. Q.; Pignatello, J. J.; Mitch, W. A. Role of black carbon electrical conductivity in mediating hexahydro-1,3,5-trinitro-1,3,5-triazine (RDX) transformation on carbon surfaces by sulfides. *Environ. Sci. Technol.* **2013**, *47*, 7129−7136.
(49) Fang, G. D.; Zhu, C. Y.; Dionysiou, D. D.; Gao, J.; Zhou, D. M. Mechanism of hydroxyl radical generation from biochar suspensions: Implications to diethyl phthalate degradation. *Bioresour. Technol.* **2015**, *176*, 210−217.
(50) Cayuela, M. L.; Sanchez-Monedero, M. A.; Roig, A.; Hanley, K.; Enders, A.; Lehmann, J. Biochar and denitrification in soils: when, how much and why does biochar reduce N_2O emissions? *Sci. Rep.* **2013**, *3*, 1732.
(51) Alburquerque, J. A.; Sanchez-Monedero, M. A.; Roig, A.; Cayuela, M. L. High concentrations of polycyclic aromatic hydrocarbons (naphthalene, phenanthrene and pyrene) failed to explain biochar's capacity to reduce soil nitrous oxide emissions. *Environ. Pollut.* **2015**, *196*, 72−77.
(52) Oh, S. Y.; Son, J. G.; Chiu, P. C. Biochar-mediated reductive transformation of nitro herbicides and explosives. *Environ. Toxicol. Chem.* **2013**, *32*, 501−508.

DOI: 10.1021/es5061512
Environ. Sci. Technol. 2015, 49, 5645−5653